Modeling field evaporation degradation of metallic surfaces by first principles calculations: A case study for Al, Au, Ag, and Pd

IOP Conf. Series: Journal of Physics: Conf. Series **1043** (2018) 012039 doi:10.1088/1742-6596/1043/1/012039

Modeling field evaporation degradation of metallic surfaces by first principles calculations: A case study for Al, Au, Ag, and Pd

Teresita Carrasco[1], Joaquín Peralta[1], Claudia Loyola[1] and Scott R Broderick[2]

[1]Departamento de Física, Facultad de Ciencias Exactas, Universidad Andrés Bello, Sazié 2212, piso 7, Santiago, Chile.
[2]Dept. of Materials Designs and Innovation-University at Buffalo: State University of New York, USA.

E-mail: joaquin.peralta@unab.cl

Abstract. Under the effects of an extreme electric field, the atoms on a metallic surface evaporate by breaking their bonds with the surface. In this work, we present the effects of a high electric field, by the use of computational simulations, for different metallic surface chemistries: Al, Au, Ag, and Pd. To model this bond breaking procedrure (i.e. field evaporation), we use density functional theory through the Quantum-Espresso (QE) simulation package, which incorporates the electric fields by adding a saw-like funcion into the Hamiltonian. This approach, known as dipole correction, was applied to all simulations as is implemented in the QE package. In this work, we calculate the evaporation field (F_e) for all metallic species, which corresponds to the mean field at which atoms can break their bonds from the surface and evaporate. This result is compared with experimantal data from Atom Probe Tomography (APT) and computational data from prior simulations.

1. Introduction

The presence of high electric fields on the order of a hundred MeV/m is becoming increasingly common as science and engineering continues to push characterization boundaries. These kinds of electric fields are observed in particle accelerators, field emission microscopes, field ion microscopes, and atom probes, among others [1, 2, 3, 4]. The presence of these high electric fields on the surface induces the field evaporation phenomena on the surface. The field evaporation phenomena on a metal surface, in which atoms are evaporated under the effects of high electric fields, were first reported by Müller on a specimen tip in a Field Ion Microscope [2]. Nowadays, field evaporation plays a crucial role in Atom Probe Tomography experiments [5] and theory [6]. Also there is a growing relevance of this phenomena on computational simulations based on first-principles, and the link between simulated F_e values and experimental results [7, 8, 9, 10, 11], alongside the variety of atomic effects on the surface triggered by field evaporation that can be analyzed with this technique. The F_e plays an important role, particularly in the reconstruction process of the experimental data provided by APT experiments, and it is well established that preferential evaporation plays an important role in the quantitative interpretation of atom probe images [12, 13, 14, 15].

Field evaporation is usually considered as a thermally activated process [7, 9] in which the ion escapes over a potential barrier. The height of the activation energy (Q) for field evaporation is dependent on the electric field(F) and decreases with increasing field strength, as shown in Figure 1. As the external electric field increases from zero, the activation energy (Q) decreases and is accompanied by the formation of a hump. The electric field at which the hump just disappears is called the critical evaporation field (F_e) at 0K. Two principle models to describe the process have been deeply studied, (a) the classical image hump, and (b) the non-classical charge-draining hump [16, 17]. Multiple limitations are associated with these models. The classical image-hump model is not applicable to field evaporation [16], as the hump is almost always assumed to be physically a charge-draining hump. On the other hand, when the ad-atom is evaporated, the overall charge around the ad-atom decreases, and the atoms are expected to be positive ions; however, due to the nature of density functional theory (DFT) [18], the charge state of the evaporating atoms cannot be determined exactly by using the conventional formalism [9].

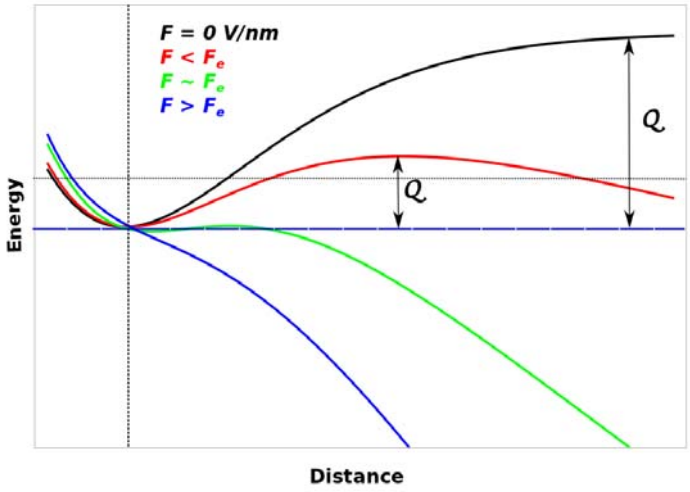

Figure 1. Schematic potential energy for pulling out an atom as a function of distance to the surface of the sample. The energy barrier Q decreases with increasing electric field. The black line represents the potential energy when there is no electric field. The red line represents the potential energy when electric field F is less than the critical evaporation field F_e, and the energy barrier decreases and is accompanied by the formation of a hump. The green line represents the potential energy when F is very close to F_e; this is the field at which the energy barrier (i.e., the hump) disappears. Finally, the blue line represents the potential energy when F greater than F_e is applied (please view color online). For all curves, zero energy is chosen at the equilibrium position of the ad-atom.

This work provides a value of the evaporation field F_e for four different metallic surfaces: Al, Au, Ag, and Pd. The values are obtained through DFT, which is one of the most relevant techniques used to understand phenomena at the atomic level because it is able to incoporate the atomic core, valence electrons, and relativistic effects in the process. Our results are compared with experimental data from APT and computational data from prior simulations [10, 7]. In our work, two different surface orientations for each surface, $< 111 >$ and $< 100 >$, have been considered.

In this paper the F_e obtained for different metallic surfaces is correlated to experimental and simulation results. We use DFT calculations to model the energetics of field evaporation

based on our previously developed methodology [10]. the rest of the document is organized as follows: The next section gives a description of the computational procedure used in the simulations; Section 3 shows the results for all of the metallic surfaces; and finally section 4 presents a discussion and conclusions of our work, along with future scopes.

2. Computational procedure

The surfaces of all different metallic compounds were built using 25 and 21 atoms for $< 111 >$ and $< 100 >$ directions, respectively. Figure 2 shows a representative structure for gold in the $< 111 >$ direction. All slabs were located in the middle of a supercell with a vacuum region of 15Å to the borders of the supercell in the z-axis. The structure sizes were considered smaller than other simulations, which have effects related to the periodicity of the cell and size. This allow us to simulate a large amount of data, as described in a previos work [10], and can take 8 to 10 times the regular time of a DFT simulation dye to the incorproation of a high electric field. In spite of this, the behavior of the field evaporation F_e for all the metallic compounds compares favorably with the reconstruction values.

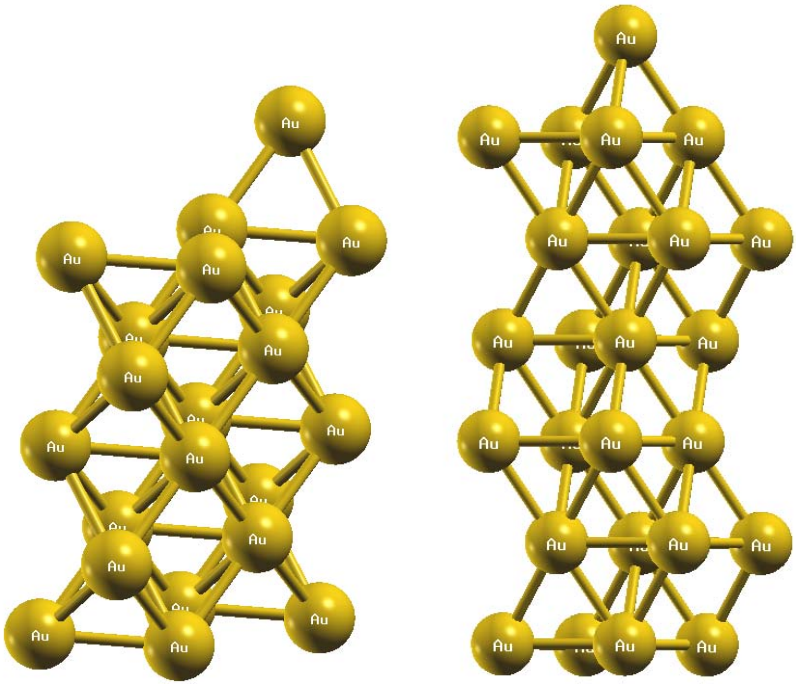

(a) Au 100 (b) Au 111

Figure 2. Representative (a) $< 100 >$/Au and (b) $< 111 >$/Au surface structures with an ad-atom on the surfaces in the $z-$direction.

The computational simulations were all performed using the Quantum-Espresso code [19] (QE) under the generalized gradient approximation (GGA). Metallic atoms were all represented by the Vanderbilt ultrasoft pseudopotential scheme. Convergence of energy and k-point mesh size were evaluated for each case. The energy cut-off used for each atomic species was 25, 40, 25, and 35 Rydberg for Ag, Al, Au, and Pd, respectively The k-point number used was 12x12x12 for the Au case and 8x8x8 for all of the rest. The Marzari-Vanderbilt [20] scheme was used for the simulations. The electric field was incorporated as an additional term in the Hamiltonian and was applied to all simulations using the dipole correction [21], implemented in the QE package.

In order to build the initial surfaces, we calculated the lattice parameters of all the metals by using the Bulk modulus. To proceed, a hydrostatic compression and expansion was used on a single lattice of each metal. With this information, we are able to determine the energy variation versus volume. With the results, we obtain the bulk modulus by fitting to the Murnaghan's equation of state [22]. The determined cell parameters and bulk modulus are presented in table 1.

Table 1. Calculation of bulk modulus B and lattice parameter a, as compared with data provided by other experimental and theoretical works.

Metal	B[GPa] [23]	B[GPa]This work	a[Å] [24]	a[Å] This work
Ag	0.69	0.61	4.085	4.149
Al	0.47	0.46	4.049	4.056
Au	0.99	0.86	4.078	4.174
Pd	1.25	1.13	3.890	3.964

The parameters are in good agreement with experimental results [25] and with previous first principles simulations [26, 10]. These results were used to build the initial structures. Four different slabs for $< 111 >$ and $< 100 >$ directions were built. They are composed of five layers, with an additional ad-atom on the surface. The direction perpendicular to the surface was chosen as the z direction. The slab was placed in the middle of a super-cell along the z direction and the vacuum spaces between the slab and the super-cell boundaries are equivalent to 15Å. All the structures (surfaces with ad-atoms) were relaxed with an ionic relaxation process, by the bfgs quasi-newton method without cell variation. The convergence criteria was set under the condition that the atomic forces on every atom are lower than 1.0×10^{-3} (in atomic units) for all directions.

As a function of the position of the ad-atom on the surface, the total energy of the system (surface and ad-atoms) was calculated under the influence of 12 different electric fields ranging from 0 to 49V/nm for Au and 0 to 27 V/nm for all other cases. The displacement of the ad-atom has been realized between -0.8Å and 6.0Å from the equilibrium position of the ad-atom. A seven-parameter function [7], at equation 1, was adopted here to fit the energy curve for the system formed by the evaporating atom and the slab under a particular electric field. In this equation, z is the position of the ad-atom, and a to h are parameters determined numerically.

$$E(z) = (a + bz + cz^2 + dz^3) \exp(-fz) + g + hz \tag{1}$$

F_e for each metallic surface has been calculated using a previously developed methodology [10]. We determined the variations of the hump-height in the presence of different electric fields (F). A sigmoid function, as shown in equation 2, has been used to fit the behavior of the hump-height under the effects of different electric fields, which have been shown to be a standard funtion in the phenomena [27, 10]. By numerical fit to the equation 2, we can evaluate the field evaporation value F_e for each type of metal surface.

$$H(F) = a + \frac{k - a}{(1 + q \exp(-b(F - m)))^{(1/n)}} \tag{2}$$

The following section shows the results for energies as a function of the ad-atom displacement and the evaporation field for each atomic configuration, and the conection of this with the F_e value.

3. Results

3.1. Evaporation Fields

A representative figure of the energy as a function of the displacement of the ad-atoms is presented. Figure 3 shows the energy required for evaporating an Au ad-atom from a $< 111 >$/Au surface as a function of the position of the ad-atom; wherein, each curve indicates a given electric field. The curves have been displaced in order to have better visual inspection of how the energy barrier decreases with increasing external electric field values.

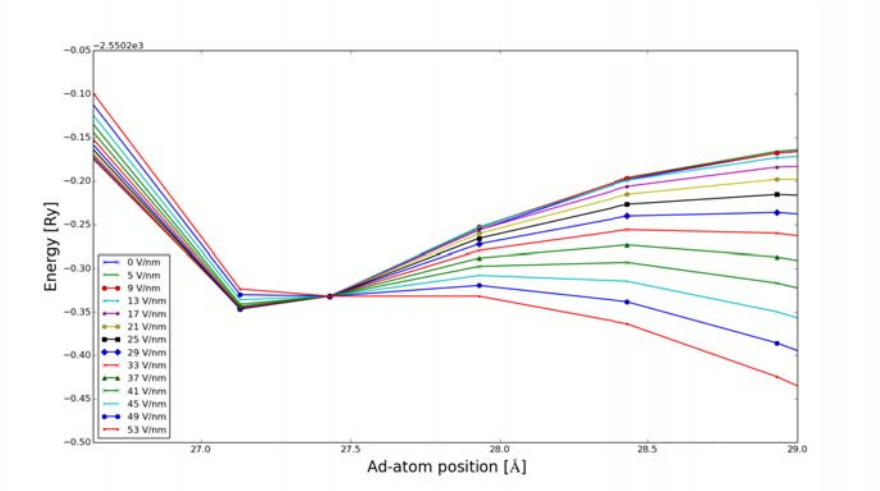

Figure 3. Energy as a function of the position of the ad-atom. Each curve represent a different intensity of the electric field. In order the electric field increases we observe the hump disappear, at the time hump completely disappear, then the ad-atom on the surface is evaporated.

A similar process is made for all different metallic surfaces in the direction $< 111 >$. For each curve, a fitting process of the data with equation 1 is used. A numerical analysis helps us to determine the the maximum and minimum of each curve in order to evaluate the hump in the sample. The results for all $< 111 >$ surfaces are presented in Figure 4.

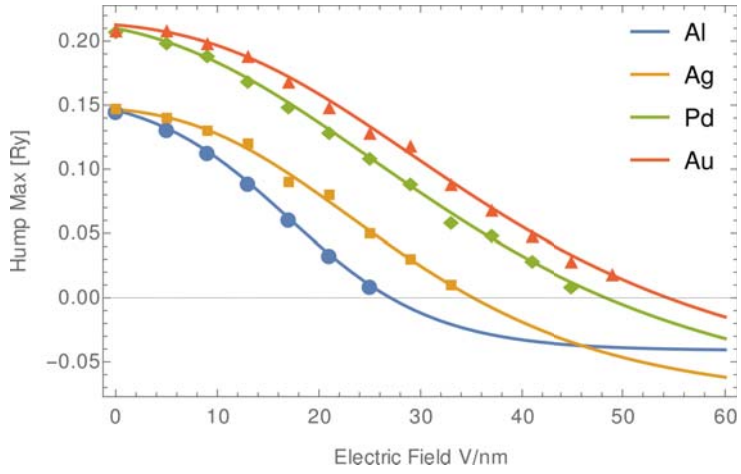

Figure 4. Energy as a function of the position of the ad-atom. Each curve represents a different intensity of the electric field. The electric field increases as we observe the hump disappear, and at the time the hump completely disappears then the ad-atom on the surface is evaporated.

The Figure 4 shows the variation of the hump in the ad-atom energy bond as the electric field is increased. The values of field evaporation for each case correspond to the zero hump for each curve for Al, Ag, Pd, and Au. We obtain F_e values of 27, 36, 48, and 54 V/nm respectively. In the particular case of Al, the lowest field evaporation observed is larger than expected. It has been shown in a previous work [10] that the largest slabs geometries result in lower field evaporation than the value obtained in the present work, and even lower than the regular value used for the reconstruction process (21 V/nm) in experiments. This means that the very local neighborhood of the ad-atom is responsible for the field evaporation necessary to remove the atom, and the effects of the periodicity based on the used methodology affects the field evaporation value, despite the distance between the atoms. It is also expected that vacancies, steps, or different ad-atom configurations modify this value [11].

For the case of $< 100 >$ surfaces, a similar procedure as previously described was made in order to obtain the variation of the hump for each metallic surface. Figure 5 presents the results of the variation of the hump for this case.

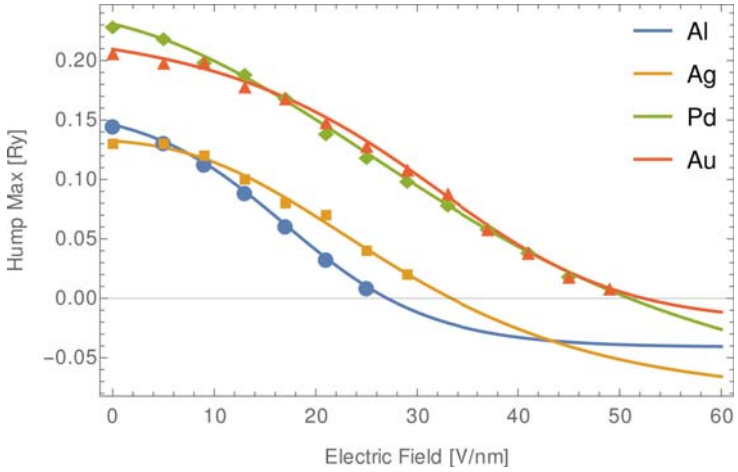

Figure 5. Energy as a function of the position of the ad-atom. Each curve represents a different intensity of the electric field. In order: the electric field increases, we observe the hump disappear, then the time hump completely disappears, and finally the ad-atom on the surface is evaporated.

As in the previous case for the $< 111 >$ direction, a clear order of the different metals is observed for the F_e: Au > Pd > Ag > Al. The table 2 shows the F_e for the different surfaces and the values used as a reference in the reconstruction process in the experimental procedures.

We observe a clear difference established between the determined values provided from the DFT procedure and the reference values for the reconstruction. However, the procedure for small size surfaces is still a good representation of the magnitude of order for all of the materials. This ordering of the evaporation fields has been attempted previously [27]; in that case, the values were almost correct with the exception of the ordering of Au and Pd. In our case, with the methodology described, we are able to reproduce the order as expected. It also has been well demostrated that the values obtained by this technique typically overestimates the values of F_e which are evaporated mostly from pristine surfaces [7, 10, 11] and do not consider the presence of imperfections at the surface like vacancies, steps, and grain boundaries, among others. For all cases, no difference larger than 3 V/nm is observed, which is larger for the Au and Pd cases.

Table 2. F_e values obtained for two different surfaces and four different metallic species. Despite the similar values for the two directions, there are still important differences in the cases of Pd. Comparison shows a clear difference with references taken from the values used in the reconstruction process.

Metal	F_e for $< 111 >$	F_e for $< 100 >$	Ref F_e
Ag	35	33	24
Al	27	27	19
Au	54	52	53
Pd	48	51	37

4. Conclusions

A well established process is used to estimate the critical evaporation field of a (111) and (100) oriented surface for four different metallic specimen: Al, Ag, Pd, and Au. A critical evaporation field (F_e) is obtained using the proposed approach. The estimated evaporation field shows differences with previos simulations based on the size of the surfaces used. Additionally, it is well-known that differences are expected because of the use of pristine surfaces which omit the presence of imperfections at the surface. Despite the differences in the comparison of each F_e, which is motivated by simulation times using the incorporation of high electric fields, a behavior congruent with all metals is observed and easily related to the reconstruction field parameter (F) with all metals. We observe also how this methodology reproduces the expected order for each metal in terms of F_e, and how the changes for different directions do not strongly affect the values necessary to evaporate the atoms.

Acknowledgements

This work was supported by the Proyecto FONDECYT Iniciación 11130501. JP Also acknowledges partial support from Proyecto FONDECYT Regular 1140514 and Proyecto UAB-775. CL acknowledges support from Proyecto FONDECYT Iniciación 11150279, Proyecto PAI-79140025, and Proyecto DI-1350-16/R.

References

[1] Grudiev A, Calatroni S and Wuensch W 2009 *Phys. Rev. ST Accel. Beams* **12**(10) 102001 URL http://link.aps.org/doi/10.1103/PhysRevSTAB.12.102001
[2] Müller E W and Bahadur K 1956 *Phys. Rev.* **102**(3) 624–631 URL http://link.aps.org/doi/10.1103/PhysRev.102.624
[3] Mller E W 1966 *The Physics Teacher* **4** 53–56 (*Preprint* http://dx.doi.org/10.1119/1.2350901) URL http://dx.doi.org/10.1119/1.2350901
[4] Kelly T F and Larson D J 2012 *Annual Review of MAterials Research* **42** 1–31
[5] Kelly T F, Vella A, Bunton J H, Houard J, Silaeva E P, Bogdanowicz J and Vandervorst W 2014 *Current Opinion in Solid State and Materials Science* **18** 81 – 89 ISSN 1359-0286 URL http://www.sciencedirect.com/science/article/pii/S1359028613000983
[6] Silaeva E P, Karahka M and Kreuzer H 2013 *Current Opinion in Solid State and Materials Science* **17** 211 – 216 ISSN 1359-0286 atom Probe Tomography URL http://www.sciencedirect.com/science/article/pii/S1359028613000685
[7] Sánchez C G, Lozovoi A Y and Alavi A 2004 *Molecular Physics* **102** 1045–1055
[8] Ono T and Hirose K 2004 *Journal Applied Physics* **95** 1568–1571‘
[9] Ono T, Sasaki T, Otsuka J and Hirose K 2005 *Surface Science* **577** 42–46
[10] Peralta J, Broderick S and Rajan K Mapping energetics of atom probe evaporation events through first principles calculations. submitted to Ultramicroscopy.

[11] Loyola C, Peralta J, Broderick S R and Rajan K 2016 *Journal of Vacuum Science & Technology A: Vacuum, Surfaces, and Films* **34** 061404 (*Preprint* http://dx.doi.org/10.1116/1.4964833) URL http://dx.doi.org/10.1116/1.4964833
[12] Marquis E A and Vurpillot F 2008 *Microscopy and Microanalysis* **14** 561–570
[13] Miller M K 1987 *Journal de Physique Colloques* **48** 565–570
[14] Philippe T, Gruber M, Vurpillot F and Blavette D 2010 *Microscopy and Microanalysis* **16** 643–648
[15] Vurpillot F, Bostel A and Blavette D 2000 *Applied Physics Letters* **76** 3127–3129
[16] Gomer R 1994 *Surface Science* **1** 129–152
[17] Forbes R G 1995 *Applied Surface Science* **87** 1–11
[18] Hohenberg P and Khon W 1964 *Physical Review* **136** B864–B871
[19] Giannozzi P, Baroni S, Bonini N, Calandra M, Car R, Cavazzoni C, Ceresoli D, Chiarotti G L, Cococcioni M, Dabo I, Corso A D, Fabris S, Fratesi G, de Gironcoli S, Gebauer R, Gerstmann U, Gougoussis C, Kokalj A, Lazzeri M, Martin-Samos L, Marzari N, Mauri F, Mazzarello R, Paolini S, Pasquarello A, Paulatto L, Sbraccia C, Scandolo S, Sclauzero G, Seitsonen A P, Smogunov A, Umari P and Wentzcovitch R M 2009 *Journal of Physics: Condensed Matter* **21** 395502 (19pp)
[20] Marzari N, Vanderbilt D and Payne M 1997 *Physical Review Letters* **79** 1337–1340
[21] Bengsston L 1999 *Physical Review B* **59** 12301–12304
[22] Murnaghan F D 1944 *Proceedings of the National Academy of Sciences* **30** 244–247 URL http://dx.doi.org/10.1073/pnas.30.9.244
[23] Sutton A P and Chen J 1990 *Philosophical Magazine Letters* **61** 139–146 (*Preprint* http://dx.doi.org/10.1080/09500839008206493) URL http://dx.doi.org/10.1080/09500839008206493
[24] each reference visit the website F 2016 We the references provided for each element in http://www.webelements.com
[25] Harada Y and Hunand D C 2002 *Materials Science and engineering A-Structural materials properties microstructure and processing* **329** 686–695
[26] Wang J Y and Zhou Y C 2004 *Physical Review B* **69** 144108–1 144108–13
[27] Sánchez C G and Lozovoi A Y Field evaporation of adatoms from metal surfaces - personal communication. personal communication.